UCSF

UC San Francisco Previously Published Works

Title

Rational design of a monomeric and photostable far-red fluorescent protein for fluorescence imaging in vivo

Permalink

Journal

ISSN

Authors

Yu, Dan
Dong, Zhiqiang
Gustafson, William Clay
et al.

Publication Date

DOI

Peer reviewed

ACCELERATED COMMUNICATIONS

Rational design of a monomeric and photostable far-red fluorescent protein for fluorescence imaging *in vivo*

Dan Yu,[1] Zhiqiang Dong,[2,3] William Clay Gustafson,[4] Rubén Ruiz-González,[5] Luca Signor,[6] Fanny Marzocca,[6] Franck Borel,[6] Matthew P. Klassen,[7] Kalpana Makhijani,[1] Antoine Royant,[6,8] Yuh-Nung Jan,[7] William A. Weiss,[4,9] Su Guo,[2]* and Xiaokun Shu[1]*

[1]Department of Pharmaceutical Chemistry, Cardiovascular Research Institute, University of California – San Francisco, San Francisco, California

[2]Department of Bioengineering and Therapeutic Science, Eli and Edythe Broad Center of Regeneration Medicine and Stem Cell Research, Institute of Human Genetics, University of California, San Francisco, California

[3]College of Life Sciences and Technology, Huazhong Agricultural University, Wuhan 430070, China

[4]Department of Pediatrics, Departments of Neurology and Neurological Surgery, University of California – San Francisco, San Francisco, California

[5]Institut Químic De Sarrià, Universitat Ramon Llull, via Augusta 390, Barcelona, 08017, Spain

[6]Institut De Biologie Structurale (IBS), University of Grenoble Alpes, CNRS, CEA, Grenoble, F-38044, France

[7]Howard Hughes Medical Institute, Department of Physiology, University of California – San Francisco, San Francisco, California

[8]European Synchrotron Radiation Facility, Grenoble, F-38043, France

[9]Helen Diller Family Comprehensive Cancer Center, University of California – San Francisco, San Francisco, California

Abstract: Fluorescent proteins (FPs) are powerful tools for cell and molecular biology. Here based on structural analysis, a blue-shifted mutant of a recently engineered monomeric infrared fluorescent protein (mIFP) has been rationally designed. This variant, named iBlueberry, bears a single mutation that shifts both excitation and emission spectra by approximately 40 nm. Furthermore, iBlueberry is four times more photostable than mIFP, rendering it more advantageous for imaging protein dynamics. By tagging iBlueberry to centrin, it has been demonstrated that the fusion protein labels the centrosome in the developing zebrafish embryo. Together with GFP-labeled nucleus

and tdTomato-labeled plasma membrane, time-lapse imaging to visualize the dynamics of centrosomes in radial glia neural progenitors in the intact zebrafish brain has been demonstrated. It is further shown that iBlueberry can be used together with mIFP in two-color protein labeling in living cells and in two-color tumor labeling in mice.

Introduction

Near-infrared fluorescent proteins (IFPs) derived from bacterial phytochromes (BphPs) expand the palette of GFP and its red homologs, which have been widely used in protein and cell labeling.[1,2] IFPs absorb at around 690 nm and GFP-like FPs absorb from ultraviolet (UV) up to 610 nm.[3–8] While IFP-derived blue-shifted mutants (e.g., iRFP670) bridges the spectral gap between GFP-like FPs and IFPs,[5] they are dimeric and thus are not ideal in protein labeling that requires the FP to be monomeric so that it does not perturb stoichiometry of the protein of interest. Based on structural and sequence analysis, we recently identified a naturally monomeric BphP and engineered it into a monomeric IFP (mIFP), which is advantageous to the dimeric BphP-derived IFPs in protein labeling, with no observable perturbation to the location or function of approximately 30 mIFP-tagged proteins.[3] To expand the FP palette for protein labeling, we decide to design a blue-shifted mutant of mIFP.

BphPs belong to the phytochrome (Phy) red/far-red photoreceptor superfamily.[9,10] In addition to BphPs, the Phy superfamily also includes plant phytochromes (Phys), cyanobacterial phytochromes (Cphs), and fungal phytochromes (Fphs).[11,12] The Phy superfamily utilizes a covalently bound tetrapyrrole bilin to sense red and far-red light, which allows the organism to adapt to changes of light environment. Cphs incorporate phycocyanobilin (PCB) as the chromophore. Lagarias *et al.* first showed that the non-fluorescent Cph1 can be engineered into a fluorescent tag, though PCB does not exist in mammalian cells.[13] BphPs use a linear tetrapyrrole bilin, biliverdin (BV), which is a catabolic metabolite of heme by heme oxygenase (HO) and is an endogenous molecule in mammalian cells.[8,14] BphPs autocatalytically incorporate the bilin chromophore. BV binds to GAF domain non-covalently and forms a thioether bond between its A-ring vinyl group and a conserved cysteine 18 (C18) at N-terminal region [Fig. 1(a)].[4,15] Upon light excitation, the D-ring of BV rotates, which results in conformational change of the protein and leads to cell signaling.[9,10] Introduction of multiple mutations around the D-ring limits its rotation and rigidifies the chromophore, which leads to fluorescence of mIFP.[3]

To blue shift mIFP, we analyzed interactions between the four tetrapyrrole rings of BV and the protein. Both B and C tetrapyrrole rings are deeply buried inside the protein through interaction between their propionic acid groups and nearby residues.[4,15] This interaction is presumably important for non-covalent binding of BV to the GAF domain [Fig. 1(a)]. Thus, we decided not to mutate residues surrounding the B and C rings. Instead we chose to mutate residues around the A-ring. A structural model of mIFP based on crystal structure of IFP2.0 (PDB: 4CQH) reveals that isoleucine 251 (I251) is located at a relatively symmetrical position and opposite to C18 across the BV plane [Fig. 1(a)]. Interestingly in the cyanobacterial phytochrome Cph1 (PDB: 2VEA),[16] its conserved cysteine 259 (C259), which forms a thioether bond with A-ring of PCB, is located at the equivalent position of I251 in mIFP [Fig. 1(b)]. Furthermore, in Cph1 leucine 15 (L15) is at the equivalent position of C18 in mIFP. Based on the structural analysis, we hypothesized that if we introduce a cysteine at position 251 in mIFP it might form a covalent bond with the A-ring. This may tilt the A-ring and decrease its conjugation to the rest of the chromophore, which may lead to blue shift of the spectra.

We therefore introduced a single mutation I251C into mIFP. The purified mutant appeared blue colored [Fig. 1(c)], and we thus named this mutant iBlueberry. To verify if iBlueberry covalently incorporate the chromophore, we did zinc-induced fluorescence assay [Fig. 1(d), bottom panel], which is a standard assay in characterizing covalent incorporation of bilin into phytochromes, based on the phenomena that bilin-zinc ion complex is orange fluorescent upon UV illumination.[10,17] We observed that zinc-induced orange fluorescence was at the same position as the protein band visualized by Coomassie blue staining, demonstrating that BV is covalently incorporated since the iBlueberry proteins were denatured in the assay. As a positive control, we also observed zinc-induced orange fluorescence from purified mIFP. As a negative control, we introduced a C18A mutation to mIFP so that the chromophore is no longer covalently incorporated. And we did not observe zinc-induced orange fluorescence from mIFP C18A mutant [Fig. 1(d)]. Therefore, our results suggest that iBlueberry covalently incorporates BV. To further clarify which cysteine (C251 or C18) is covalently linked to BV, we mutated C18 to an isoleucine. We observed zinc-induced orange fluorescence from the purified iBlueberry C18I mutant
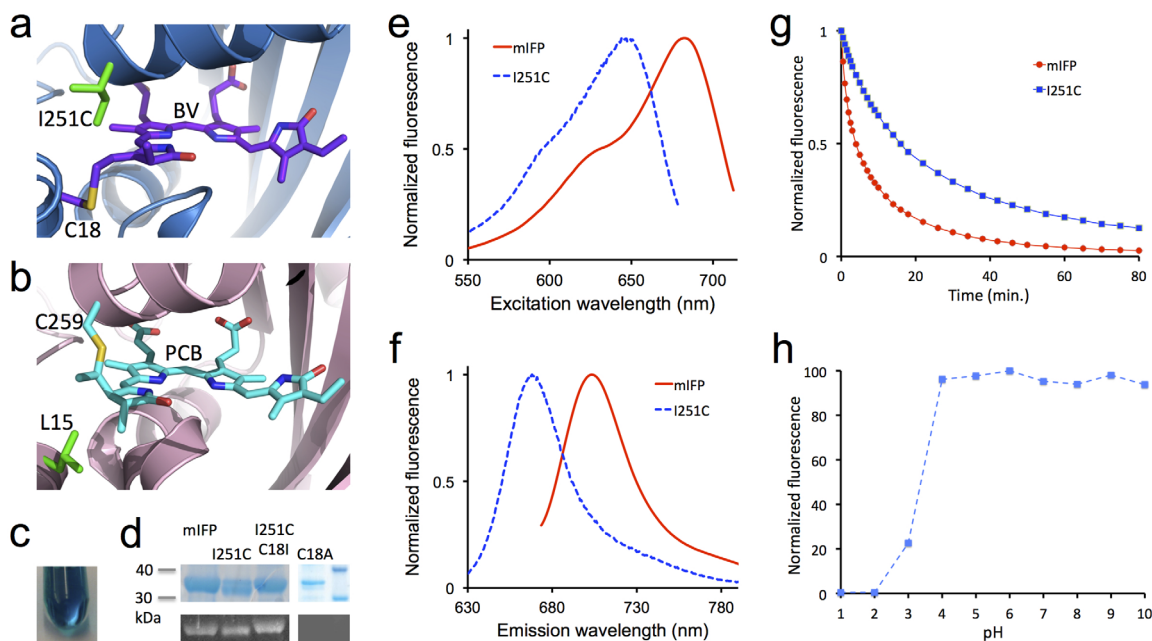
Figure 1. Rational design of a far-red fluorescent protein iBlueberry. (**a**) Modeled structure of mIFP based on IFP2.0 (PDB: 4CQH), with the single mutation I251C. The chromophore BV is shown in purple. (**b**) Structure of CphP1 (PDB: 2VEA). The chromophore PCB is shown in cyan. (**c**) Purified iBlueberry. (**d**) Coomassie blue staining and zinc-induced fluorescence assay (**bottom**) of mIFP, iBlueberry (i.e., mIFP/I251C) and other mutants. The molecular mass standards are shown on the right. (**e**) Excitation spectra of mIFP and its I251C mutant (i.e., iBlueberry). (**f**) Emission spectra of mIFP and its I251C mutant. A structure model of mIFP with introduced mutations. The chromophore BV is shown in purple. (**g**) Photobleaching of mIFP and iBlueberry (i.e., mIFP/I251C). Normalized fluorescence intensity over time under illumination of 100% 640 nm laser. The laser power is 13.4 mW and illumination light intensity is 1.83 W/cm². (**h**) Fluorescence of purified iBlueberry against pH.

(i.e., mIFP I251C/C18I mutant), which suggests that C251 forms a covalent bond with BV.

The excitation spectra showed that iBlueberry is 39 nm blue-shifted compared with mIFP, with excitation maximum at 644 nm whereas mIFP has an excitation peak at 683 nm [Fig. 1(e)]. The emission spectra indicated that iBlueberry is 37 nm blue-shifted relative to mIFP, with emission peak at 667 nm [Fig. 1(f)]. Furthermore, the excitation spectrum of iBlueberry C18I mutant is very similar to that of iBlueberry, suggesting that the residue at position 18 has little effect on the electronic structure of the chromophore (Supporting Information Fig. 1), and thus is unlikely to form a covalent bond with the chromophore. These are consistent with the results from the zinc-induced fluorescence assay. The C18I mutation affects the emission spectrum with slight red-shift by approximately 10 nm (Supporting Information Fig. 1). The results confirm our structure-based rational strategy in blue-shifting mIFP by one single mutation. The details of the covalent bond between C251 and BV will require further studies in the future, such as X-ray crystallographic studies.

A photostable fluorescent tag is preferred for imaging protein dynamics. Photobleaching experiments demonstrated that the half-life of iBlueberry fluorescence is 15.9 min, which is four times of that of mIFP (3.9 min) [Fig. 1(g), Supporting Information

Table 1]. Therefore, iBlueberry is suitable for time-lapse fluorescence imaging of protein dynamics. The C18I mutation decreases photostability with the half-life of iBlueberry C18I 11.6 min (Supporting Information Fig. 2, Supporting Information Table 1). The fluorescence of iBlueberry is stable at a wide range of pH from 4 to 10 [Fig. 1(h)]. HEK293 cells expressing iBlueberry is homogenously fluorescent (Supporting Information Fig. 3), suggesting that iBlueberry is soluble in living cells without forming aggregation and is thus suitable to label proteins of interest.

To demonstrate iBlueberry as a protein fusion tag in living animals, we fused iBlueberry to centrin, a component of the centriole. Expression of this fusion protein correctly labeled the centrosome in living zebrafish [Fig. 2(a,b)], enabling us to observe the dynamic centrosome behavior in radial glia (RG) progenitors, the principal neural stem cells (NSCs) in the vertebrate brain.[18] Previously in the developing mouse cortical RG progenitors, centrosomes are detected in their apical endfeet at the ventricular zone (VZ) surface.[19–21] Recently, it is found that centrosomes also maintain their apical localization in developing zebrafish retinal neuro-epithelia.[22] To observe the dynamics of the apical endfoot-localized centrosome during RG progenitor division, we created a myristoylated TdTomato (Myr-TdTomato) to label the cell plasma membrane, and a nuclear
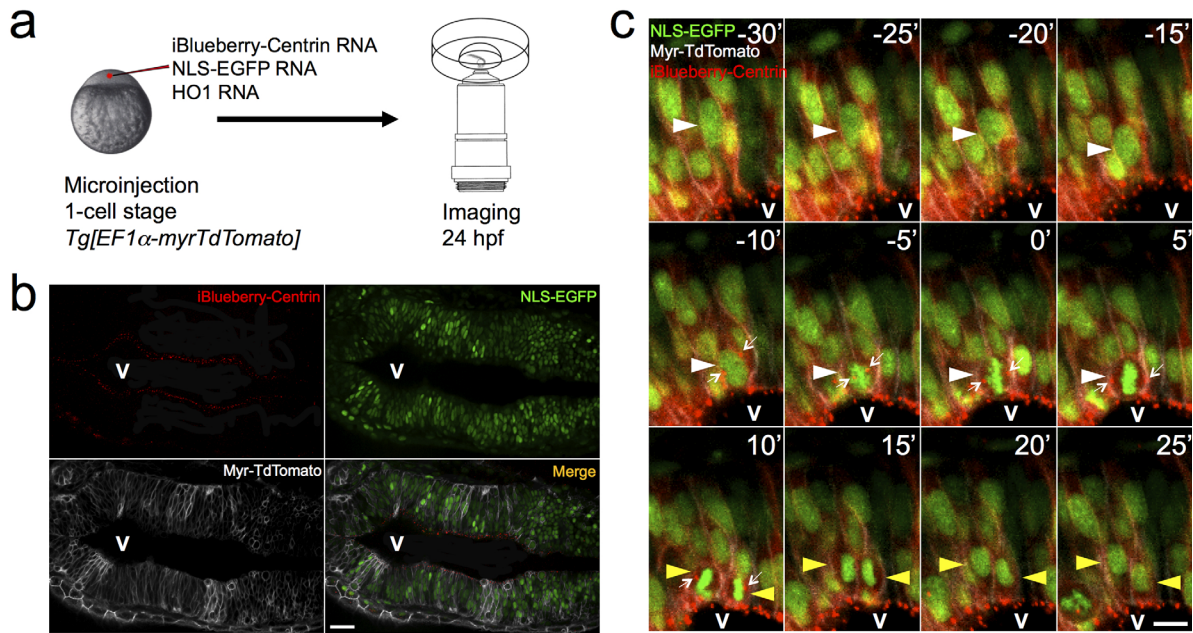
Figure 2. Centrosome dynamics in radial glia (RG) neural progenitors revealed by time-lapse *in vivo* imaging in the developing zebrafish brain. (**a**) A schematic shows the experimental design. (**b**) Representative images show that the centrosomes of RG progenitors, labeled by iBuleberry-Centrin, predominantly locate at the ventricular zone (VZ) surface. V: ventricle. Scale bar: 50 μm. (**c**) Representative montage of selected images from time-lapse *in vivo* imaging, tracking a single fluorescently labeled RG progenitor across space and time. Time "0" is defined as the time point of metaphase when the condensed chromosome is distinguishable. Minus time indicates the time before metaphase, while plus time means the time after metaphase. The mother RG progenitor undergoing division is indicated by *white arrowheads*, while the two daughter cells are indicated by *yellow arrowheads*. *Arrows* point to the two centrosomes in the dividing RG progenitor. Scale bar: 10 μm.

localization signal-tagged EGFP (NLS-EGFP) to mark the nucleus. We generated the *tg[EF1α-myrTd-Tomato]* transgenic zebrafish. Sense RNAs of iBlueberry-Centrin, NLS-EGFP, and HO1 were injected into 1-cell stage *tg[EF1α-myrTdTomato]* embryos. HO1 is used to produce BV and has no toxicity in zebrafish as demonstrated previously.[3] At 24 hours post fertilization (hpf), labeled embryos were subjected to time-lapse imaging for 6 hours to visualize spatial distribution and dynamics of the centrosome [Fig. 2(a)]. We observed that the centrosomes of RG progenitors predominantly located at the apical surface (ventricular surface) during interphase of the cell cycle [Fig. 2(b)], consistent with the observations in the developing mouse cortical RG progenitors[19–21] and in zebrafish neural rod progenitors prior to lumen formation.[23,24] We followed 52 dividing RG progenitors by time-lapse *in vivo* imaging [Fig. 2(c) and Supporting Information Movie 1]. In all 52 cases, the two centrosomes remained at the apical surface during the interphase. Since the condensed metaphase chromosome was a prominent landmark, we designated the mitotic metaphase as Time 0 in our imaging analysis [Fig. 2(c)]. We noted that around 15 min prior to the metaphase, the RG nucleus underwent a rapid descent toward the VZ surface [Fig. 2(c), −15']. Five minutes later, the two centrosomes ascended from the VZ surface to abut the prophase nucleus. Based on the centrosome posi-

tion, we could infer that the mitotic spindle plane was located approximately in parallel to the VZ surface [Fig. 2(c), −10']. As chromosomes continued to condense, the RG progenitors became more rounded [Fig. 2(c), 5']. Approximately 10 min after the metaphase, two daughter cells were born, with the centrosomes still visibly close to the new-born nuclei [Fig. 2(c), 10']. Interestingly, during the next 5 min, the centrosomes rapidly descended toward the VZ surface and remained there while the two daughter cells shifted their position, becoming a basal and an apical daughter as previously observed.[25] These results reveal the rapid movement and the striking affinity of the centrosomes toward the VZ surface in living dividing vertebrate RG progenitors. Further biological investigations are required to uncover molecular mechanisms of the spatiotemporal dynamics of the centrosome behavior.

To demonstrate that iBlueberry can be used with mIFP in two-color protein labeling in living cells, we fused iBlueberry to lifeact and mIFP to histone 2B (H2B). Expression of both fusion proteins in live HEK293 cells correctly labeled actin filaments and nucleus, respectively [Fig. 3(a)]. The fluorescence of iBlueberry and mIFP was well separated using appropriate filters (Online Methods). No exogenous BV was added nor co-expression of HO1 gene, suggesting that iBlueberry and mIFP utilized endogenous BV in HEK293 cells. This is consistent with
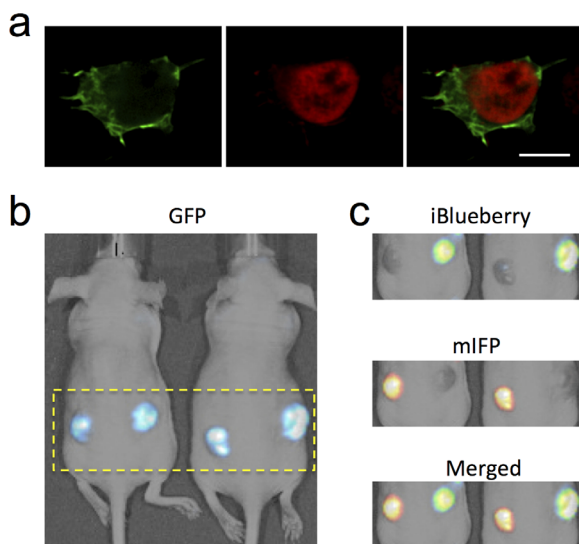
Figure 3. Two-color protein and tumor labeling using iBlueberry and mIFP. (**a**) Two-color protein labeling in living HEK293 cells: actin filaments marked by Lifeact-iBlueberry (**left**), nucleus labeled by histone 2B (H2B)-mIFP (**middle**). The merged image is shown on the right. Scale bar, 10 μm. (**b, c**) Two-color tumor labeling in mice. The tumor on the right part of the mouse body expresses iBlueberry IRES GFP, whereas the tumor on the left part expresses mIFP IRES GFP. The fluorescence from GFP (b), iBlueberry (c, **top**), and mIFP (c, **middle**) was detected using appropriate filters. See text for details.

our previous results that mIFP utilizes endogenous BV in mammalian cells.

To demonstrate that iBlueberry and mIFP can be used for two-color tumor labeling in living mice, we created stable glioblastoma cell line LN229. Both cell lines also express GFP using an internal ribosome entry site (IRES). We injected LN229 cells into mice and they grew into tumors, suggesting no or little cytotoxicity of iBlueberry and mIFP. The LN229 cells expressing iBlueberry IRES GFP were injected into the right part of the body, whereas the cells expressing mIFP IRES GFP were injected into the left part. All the tumors were green fluorescent, suggesting good expression of GFP [Fig. 3(b)]. The fluorescence from the tumor on the right part of the mouse body was detected in the iBlueberry channel with the excitation (640 ± 15 nm) and emission (680 ± 10 nm) filters optimized for iBlueberry [Fig. 3(c), top panel]. In contrast, little fluorescence from the tumor on the left part was detected in the iBlueberry channel. On the other hand, fluorescence from the tumor on the left part that expresses mIFP was detected in the mIFP channel with the excitation (670 ± 15 nm) and emission (720 ± 10 nm) filters optimized for mIFP [Fig. 3(c), middle panel]. In contrast, fluorescence from the tumor expressing iBlueberry was negligible in the mIFP channel. Therefore, iBlueberry can be used with mIFP in two-color tumor labeling in living mice [Fig. 3(c),

bottom panel]. Since no exogenous BV was injected and no HO1 gene was co-expressed, iBlueberry and mIFP seem to utilize endogenous BV in the xenografted tumor cells. iBlueberry was also expressed in the body muscle of *Drosophila* larvae with homogenous fluorescence (Supporting Information Fig. 4), suggesting that iBlueberry can be used in *Drosophila* imaging.

In summary, we have designed iBlueberry by introducing a single mutation to mIFP based on structural analysis. iBlueberry is shown to perform well as a protein tag for long-term time-lapse imaging of centrosome dynamics in living zebrafish during NSC division. iBlueberry can also be used in two-color protein and tumor labeling, expanding the FP palette for cell and molecular biology. iBlueberry is a potential candidate for developing cell signaling reporters,[26] such as the protein-fragment complementation assay[27,28] as well as FRET reporters, either as a donor paired with mIFP or as an acceptor with a GFP-like far-red FP.

Materials and Methods

Gene mutagenesis, protein purification, and characterization

The iblueberry and iblueberry_C18I were created by site-directed mutagenesis using a QuickChange Mutagenesis Kit (Stratagene). iblueberry, iblueberry_C18I, and mIFP were expressed with C-terminal polyhistidine-tag on a pBAD expression vector (Invitrogen).The following primers were used to introduce point mutation:

5′-GCCTGCGCTCTATGTCCCCGtgCCACCAGAA
ATACATGCAGGA-3′ (Forward);
5′-TCCTGCATGTATTTCTGGTGGcaCGGGGACA
TAGAGCGCAGGC-3′ (Reverse);
5′-GGCCACGCGTTTCTGGCTAACattGAACGCG
AGCAGATCCACCTG-3′ (Forward);
5′-CAGGTGGATCTGCTCGCGTTCaatGTTAGCC
AGAAACGCGTGGCC-3′ (Reverse).

Proteins were purified with the Ni-NTA purification system (Qiagen). Protein concentrations were measured by the BCA method (Pierce). The extinction coefficients were based on a comparison of absorbance values for the protein at the main peak (692 nm or 694 nm) with the absorbance value at the 391 nm peak assuming the latter to have the extinction coefficient of the free BV, which is $39,900$ M^{-1} cm^{-1}. For determination of quantum yield, fluorescence signal of iblueberry_C18I mutant and mIFP were compared with that of the equally absorbing Alexa Fluor 647 dye (quantum yield is 0.33 in PBS, Invitrogen).The pH titrations were done using a series of buffers (100 m*M* sodium

acetate, 300 mM NaCl for pH 2.5–5.0, and 100 mM NaH$_2$PO$_4$, 300 mM NaCl for pH 4.5–9.0).

Photobleaching measurements of fluorescent proteins (FPs) were performed using microdroplets of freshly purified proteins at 0.5 mg/mL in elution buffer under mineral oil on a Nikon eclipse Ti inverted spinning disk microscope equipped with a 60× NA 1.45 oil objective lens (Nikon) and controlled by NIS-Element software (Nikon Instruments). The microdroplets of the purified proteins were excited with a 640 nm laser constitutively and fluorescence were collected with a 731 ± 68.5 nm emission filter. Images were taken every 10 second for 30 min and every 1 min after. Normalized fluorescence was plotted against time.

For SDS-PAGE and Zn-induced Fluorescence Assay, purified Proteins of mIFP, iblueberry and iblueberry_C18I were resolved by SDS-PAGE using NuPAGE Novex 4%–12% (wt/wt) Bis-Tris protein gels (Life Technologies). For the Zn-induced fluorescence assay, after SDS-PAGE, the gel was soaked in 20 μM zinc acetate at room temperature for 30 min in the dark. The zinc-induced fluorescence of the BV-bound proteins was observed under UV light in an AlphaImager 3300 Imaging System (Alpha Innotech).

Fluorescent imaging in mammalian cells

For two-color imaging, mIFP was fused to N terminal of H2B and cloned into the pcDNA3.1 vector. iblueberry was fused to C terminal of Lifeact and cloned into the pcDNA3 vector. The following primers were used:

5′-ATCCGCTAGCATGTCCGTCCTGACGCCG-3′ (Forward);

5′-AGTCAGCGGTACCGACATGGTGGCGACCGG TGGATC-3′ (Reverse);

5′-GATCCACCGGTCGCCACCATGTCGGTACCG CTGACT-3′ (Forward);

5′-TCGCGGCCGCTCATTTGGACTGAGACTGTG CAA-3′ (Reverse).

HEK293A cells were transfected with mIFP-H2B and LifeAct-iblueberry using calcium phosphate transfection method and then imaged 48 h later on a Nikon eclipse Ti inverted spinning disk microscope controlled by NIS-Element software (Nikon Instruments). iBlueberry was imaged with the 640 nm laser and a 661 ± 10 nm emission filter; mIFP was imaged with the 640 nm laser and a 732 ± 34 nm emission filter. Images were processed and analyzed with ImageJ.

Stable transgenesis in zebrafish

Stable *tg[EF1α-myrTdTomato]* transgenic zebrafish line was generated using the Tol2 transposon system. Plasmid EF1α-myrTdTomato-PT2KXIG (50 pg per embryo) together with Tol2 transposase (10 pg per embryo) were injected into 1-cell stage embryos of AB wild type fish. Injected embryos were raised to adulthood (G0) and screened for germ-line transmission by crossing with AB wild type fish. The germ-line transgenic founders would yield embryos with myr-TdTomato expression, which could be easily distinguished under the epi-fluorescent microscope. The embryos with ubiquitous myrTdTomato expression were raised to adulthood (F1).

Fusion construct and RNA injection

Expression plasmids pCS2-iblueberry-zcentrin and pCS2-HO1 were created by PCR amplification of mIFP-H2B and HO1 ORF's, respectively, and then cloned into pCS2+ (gift from Stephanie Woo). The following primers were used for generation of pCS2-iblueberry-zcentrin: The following primers were used:

5′-GGTGGTGGATCCATGTCGGTACCGCTGAC-3′ (Forward);

5′-ACCACTAGACCCGCCACCGGACCCGCCACC ACTCCCGCCACCTTTGGACTGAGACTGTGC-3′(Reverse);

5′-GGGTCCGGTGGCGGGTCTAGTGGTCTCGAG ATGGCGTCCGGCTTCAG-3′(Forward);

5′-GGTGGTGAATTCTTATTAGTACAGATTGGTT TTCT-3′ (Reverse).

Capped messenger RNA was synthesized using the mMESSAGE mMACHINE SP6 kit (Ambion). RNA injections were performed at 1-cell stage. Sense strand-capped RNA was synthesized by SP6 transcription from NotI-linearized plasmid using the mMESSAGE mMACHINE system (Ambion). Sense RNAs of iBlueberry and NLS-EGFP were both injected at 400 pg per embryo.

Time-lapse in vivo imaging in zebrafish

To observe the centrosome dynamics of radial glia in zebrafish embryos, time-lapse *in vivo* imaging was performed on *tg[EF1α-myrTdTomato]* transgenic embryos injected with iBlueberry-Centrin sense RNA and NLS:EGFP sense RNA. At 24 hpf, embryos were mounted in 0.8% low melting point agarose and properly placed on a temperature-controlled stage. We used a Nikon spinning disc confocal microscope with 40× inverted objectives. Fluorescently labeled radial glia were imaged for 6 hours with a fixed interval of 5 min under a 40× water-emersion objective. The parameters of imaging were determined as sufficient to capture the centrosome dynamics, while reducing photo-bleaching during the imaging period.

***Fluorescence imaging in* Drosophila.** For expression of iBlueberry in *Drosophila*, a transcript encoding iBlueberry-T2A-HO1 was subcloned into pJFRC81 and phiC31-integrated into the genome at position 75A10 [PBac{y+-attP-9A} VK00005]. Expression of iBlueberry-T2A-HO1 in muscles was driven by Mef2.R-GAL4. F1 progeny were collected

on yeasted grape agar plates and raised at 25℃. Intact 1st Instar larvae were acutely immobilized in water during imaging using a small thermoelectric cooler (Laird, Schaumburg, IL) maintained at 4℃ by a PID Relay (Watlow, St. Louis, MO). Fluorescent images were taken with a Nikon spinning disk confocal microscope. Confocal images were acquired using a 20× (NA = 0.75) objective (Nikon) and a digital sCMOS camera (Hamamatsu) on a Nikon eclipse Ti inverted spinning disk microscope controlled by NIS-Elements software (Nikon). iBlueberry was excited by a 640 nm laser and fluorescence collected with a 731 ± 68.5 nm emission filter. Images were processed and analyzed with ImageJ. Condensation arising due to the temperature differential was mitigated by wiping a thin film of water across the coverslip.

Construction of lentiviral vectors and establishment of stable cells lines

To create Lentivirus expressing iblueberry or mIFP and GFP, a transcription unit comprising the iblueberry or mIFP coding sequence, the poliovirus IRES, and GFP was constructed by assembly PCR, cloned into pENTR1a (Invitrogen), and transferred into pLenti-CMV-DEST (Invitrogen) by Gateway recombinase (Invitrogen). The following primers were used; 5′-AAACTTAAGCTTGCCACCATGTCGGTACC GCTG-3′ (Forward); 5′-CTTGTACAGCTCGTCCATG C-3′ (Reverse). Viruses were produced in HEK293 cells with ViraPower™ Lentiviral Expression System (Invitrogen) according to the manufacturer's recommendations and purified by anion exchange chromatography (FastTrap purification kit, Millipore), resuspended in HBSS + 10% glycerol, and stored in aliquots at −80℃. Titers as assessed on HEK293 cells by GFP fluorescence were 44,000 infectious units (IU) per mL for each virus. For transfection, LN229 Cells were plated on 100 mm culture dishes and cultured to approximately 80% confluence. About 3 mL of virus aliquots and 3 mL of fresh medium were mixed and added on the cells. Long-term transgene expression was maintained by selecting for resistance to puromycin at a final concentration of 10 μg/mL.

Subcutaneous xenografts and in vivo mouse imaging

For subcutaneous injection, 4- to 6-week-old female BALB/c nu/nu mice (Harlan; Sprague–Dawley) were used. LN229 cells stably expressing iblueberry and GFP or mIFP and GFP were cultured in H21 medium containing 10% FBS, harvested in logarithmic growth, and suspended at a density of 2×10^8 cells/mL in PBS at room temperature. Cell suspensions (5 μL) containing approximately 3×10^6 LN229 cells at room temperature were injected subcutaneously into the dorsal side of each mouse ($n = 5$) with cells expressing mIFP and GFP on the left and

cells expressing iblueberry and GFP on the right. Subcutaneous xenografts were assessed weekly. Tumors were established about 2–3 weeks after injections. All mouse experimentation was performed in accordance with protocols approved by the IACUC at the University of California, San Francisco and adhered to the National Institutes of Health Guide for the Care and Use of Laboratory Animals. Mouse imaging was performed with an IVIS Spectrum instrument (Caliper LifeSciences) in epifluorescence mode equipped with a 465/30 nm excitation filter and a 520/20 nm emission filter for GFP; a 640/30 nm excitation filter and 680/20 nm emission filter for iBlueberry; and 670/30 nm excitation filter and a 720/20 nm emission filter for mIFP. Images were processed using the Living Image Software 4.0.

Author Contributions

X.S. and S.G. conceived the project. X.S., S.G., W.C.G., A.R., Y.N.J., W.A.W. planned the experiments. D.Y., Z.D., W.C.G., R.R., L.S., F.M., F.B., M.P.K., K.M. performed the experiments. X.S., S.G., D.Y., Z.D. wrote the manuscript. All the authors contributed to the final draft.

References

1. Day RN, Davidson MW (2009) The fluorescent protein palette: tools for cellular imaging. Chem Soc Rev 38: 2887–2921.
2. Tsien RY (2009) Constructing and exploiting the fluorescent protein paintbox (Nobel Lecture). Angew Chem Int Ed Engl 48:5612–5626.
3. Yu D, Baird MA, Allen JR, Howe ES, Klassen MP, Reade A, Makhijani K, Song Y, Liu S, Murthy Z, Zhang SQ, Weiner OD, Kornberg TB, Jan YN, Davidson MW, Shu X (2015) A naturally monomeric infrared fluorescent protein for protein labeling. Nat Methods 12:763–765.
4. Yu D, Gustafson WC, Han C, Lafaye C, Noirclerc-Savoye M, Ge W-P, Thayer DA, Huang H, Kornberg TB, Royant A, Jan LY, Jan YN, Weiss WA, Shu X (2014) An improved monomeric infrared fluorescent protein for neuronal and tumour brain imaging. Nature Commun 5:3626.
5. Shcherbakova DM, Verkhusha VV (2013) Near-infrared fluorescent proteins for multicolor in vivo imaging. Nat Methods 10:751–754.
6. Auldridge ME, Satyshur KA, Anstrom DM, Forest KT (2012) Structure-guided engineering enhances a phytochrome-based infrared fluorescent protein. J Biol Chem 287:7000–7009.
7. Filonov GS, Piatkevich KD, Ting L-M, Zhang J, Kim K, Verkhusha VV (2011) Bright and stable near-infrared fluorescent protein for in vivo imaging. Nat Biotechnol 29:757–761.
8. Shu X, Royant A, Lin MZ, Aguilera TA, Lev-Ram V, Steinbach PA, Tsien RY (2009) Mammalian expression of infrared fluorescent proteins engineered from a bacterial phytochrome. Science 324:804–807.
9. Giraud E, Fardoux J, Fourrier N, Hannibal L, Genty B, Bouyer P, Dreyfus B, Verméglio A (2002) Bacteriophytochrome controls photosystem synthesis in anoxygenic bacteria. Nature 417:202–205.

10. Bhoo SH, Davis SJ, Walker J, Karniol B, Vierstra RD (2001) Bacteriophytochromes are photochromic histidine kinases using a biliverdin chromophore. Nature 414:776–779.

11. Rockwell N, Su Y, Lagarias J (2006) Phytochrome structure and signaling mechanisms. Annu Rev Plant Biol 57:837.

12. Karniol B, Wagner JR, Walker JM, Vierstra RD (2005) Phylogenetic analysis of the phytochrome superfamily reveals distinct microbial subfamilies of photoreceptors. Biochem J 392:103.

13. Fischer AJ, Lagarias JC (2004) Harnessing phytochrome's glowing potential. Proc Natl Acad Sci USA 101: 17334–17339.

14. Giraud E, Verméglio A (2008) Bacteriophytochromes in anoxygenic photosynthetic bacteria. Photosyn Res 97: 141–153.

15. Wagner JR, Brunzelle JS, Forest KT, Vierstra RD (2005) A light-sensing knot revealed by the structure of the chromophore-binding domain of phytochrome. Nature 438:325–331.

16. Essen L-O, Mailliet J, Hughes J (2008) The structure of a complete phytochrome sensory module in the Pr ground state. Proc Natl Acad Sci USA 105:14709–14714.

17. Berkelman TR, Lagarias JC (1986) Visualization of bilin-linked peptides and proteins in polyacrylamide gels. Analyt Biochem 156:194–201.

18. Kriegstein A, Alvarez-Buylla A (2009) The glial nature of embryonic and adult neural stem cells. Annu Rev Neurosci 32:149–184.

19. Wang X, Tsai J-W, Imai JH, Lian W-N, Vallee RB, Shi S-H (2009) Asymmetric centrosome inheritancemaintains neural progenitors in theneocortex. Nature 461:947–955.

20. Chenn A, Zhang YA, Chang BT, McConnell SK (1998) Intrinsic polarity of mammalian neuroepithelial cells. Mol Cell Neurosci 11:183–193.

21. Hinds JW, Ruffett TL (1971) Cell proliferation in the neural tube: an electron microscopic and golgi analysis in the mouse cerebral vesicle. Z Zellforsch Mikrosk Anat 115:226–264.

22. Strzyz PJ, Lee HO, Sidhaye J, Weber IP, Leung LC, Norden C (2015) Interkinetic nuclear migration is centrosome independent and ensures apical cell division to maintain tissue integrity. Dev Cell 32:203–219.

23. Buckley C, Clarke J (2014) Seminars in cell and developmental biology. Semin Cell Dev Biol 31:100–105.

24. Buckley CE, Ren X, Ward LC, Girdler GC, Araya C, Green MJ, Clark BS, Link BA, Clarke JDW (2013) Mirror-symmetric microtubule assembly and cell interactions drive lumen formation in the zebrafish neural rod. Embo J 32:30–44.

25. Dong Z, Yang N, Yeo S-Y, Chitnis A, Guo S (2012) Intralineage directional notch signaling regulates self-renewal and differentiation of asymmetrically dividing radial glia. Neuron 74:65–78.

26. To T-L, Piggott BJ, Makhijani K, Yu D, Jan Y-N, Shu X (2015) Rationally designed fluorogenic protease reporter visualizes spatiotemporal dynamics of apoptosis in vivo. Proc Natl Acad Sci USA 112:3338–3343.

27. Tchekanda E, Sivanesan D, Michnick SW (2014) An infrared reporter to detect spatiotemporal dynamics of protein- protein interactions. Nat Methods 11:641.

28. Filonov GS, Verkhusha VV (2013) A near-infrared BiFC reporter for in vivo imaging of protein-protein interactions. Chem Biol 302:221–278.